Effect of Heating Rate on the Kinetics of Martensitic Transformation of Ni-Ti-Hf alloys using Differential Scanning Calorimetry (DSC)

Glauco R. de F. Brito[a]* [iD], *Walman B. de Castro[a]* [iD], *Roniere L. Soares[b]* [iD]

[a]Universidade Federal de Campina Grande, Departamento de Engenharia Mecânica, Campina Grande, PB, Brasil.
[b]Universidade Federal de Campina Grande, Departamento de Engenharia de Produção, Campina Grande, PB, Brasil.

The transformation martensite-austenite and Kinetics in Ni-Ti-Hf shape memory alloys (SMAs) were calculated for the first time. The Johnson- Mehl – Avrami- Komogorov (JMAK) equation was used to simulate the transformation Martensite- Austenite, which exhibited the same trends as the DSC test results. DSC studies were conducted using four different heating rates to study the kinetics of the thermally induced transformation process and the dependence of the kinetic parameters and the heating rate. It was clarified that the heating rate adjusts the enthalpies of transformation, indicating that the heating rate can be used to adjust the phase change parameter. The Arrhenius method was used to calculate the activation energies, and it was observed from its use that the activation energies increase as there is an increase in the ternary element in the composition. Moreover, using the same heating is a valuable means of comparing activation energies for the same alloy system. This study provides a reference for designing and calculating the kinetics of Ni- Ti- Hf high-temperature shape memory alloys.

Keywords: *Shape Memory Alloys, Kinetic Transformation, Differential Scanning Calorimetry, High-Temperature Shape Memory Alloys.*

1. Introduction

Shape memory alloys (SMA) have been widely used in engineering applications in the most diverse fields, from the biomedical industry to the aerospace industry, thanks to their ability to recover their initial shape from the application of an adequate thermal cycle due to the shape memory effect (SME) and recovery from large deformations induced by mechanical loading (SE) Superelasticity[1].

The shape memory alloys developed in the nickel titanium system constitute one of the largest groups concerning the possible arrangements (compositions) of alloys with intrinsic property shape memory effect (SME)[2]. This feature confers a high degree of industrial applicability to these alloys, as it allows manufacturing through these spring alloys capable of thermoactivated industrial actuators with a high capacity for shape recovery[3,4]. One of the essential properties of shape memory alloys in the nickel titanium system is their high resistance to oxidation, which makes these alloys of great importance for the construction of biomedical elements (prostheses)[4,5].

However, it is observed that the nickel titanium binary system alloys have a limiting singularity regarding their use for applications at high temperatures when under high thermal demands. These alloys perform phase transformations at relatively low transformation temperatures compared to alloys composed of ternary elements added to improve this variable[2]. Alloys with higher transformation temperatures belong to a specific subgroup of shape memory alloys known as High-Temperature Shape Memory Alloys (HTSMAs)[6]. These alloys are the only shape memory alloys with transformation temperatures above one hundred degrees Celsius and can operate under high-temperature conditions[7,8].

Adding a particular ternary element to Ni-Ti starting binary can increasetransformations temperatures of alloys[9,10]. At the microstructural level, it can be stated from the literature developed on HTSMAs, that the possibility of a ternary element supplanting the transformation of an SMA into an HTSMA concerns the character of this third element allocated to the binary has a high temperature in the melting point (Tm > 1000°C). However, it is observed that the increase in temperatures oftransformations in HTSMA alloys from nickel titanium systems is probably also related to the fact that the atomic radius and the melting point of the third element are more significant than nickel and titanium[11].

Analyzing, in particular, the HTSMAs achieved based on the addition of the ternary element hafnium to the initial binary nickel titanium, the increase in transformation temperatures can also be approached by observing the microstructural character of the alloys of the nickel titanium system plus the ternary element hafnium[8,10]. In this case, this reality becomes observable since the atomic radius of hafnium is r = 0.155 nm and has a melting point of Tm = 2232.85 °C, while nickel has an atomic radius of r = 0.124 nm and a melting point temperature of Tm = 1454.85 °C, in the same direction, titanium has an atomic radius of order r = 0.140 nm and melting point temperature at Tm = 1667.85°C[12].

*e-mail: glaucoruben@hotmail.com

To analyze the effect of increasing hafnium contents in the NiTiHf alloys used in this work, we will use DSC (Differential Scanning Calorimetry) technology to characterize. A critical correlation studied in this work, and perfectly translatable using the DSC, refers to the possibility that the properties of SMAs are affected by heating rates during phase transformations[13,14]. In this context, the Differential Calorimeter Scanner (DCS) is used to measure the thermal activity of the physical properties of SMA[14].

In this work, two kinetic models strongly supported in the literature were used to confirm the behavioral trends of the physical properties of these alloys – in terms of thermal activity – empirically captured by DSC. To determine the precision between the kinetic model and the empirical measurements, as well as the description of the character of the kinetic transformation from its coefficient, the Avrami model will be used[15-17]. The Arrhenius model will investigate activation energies for the martensite-austenite transformation process[6,18-20].

2. Experimental Procedure

2.1. Description

The compositions obtained and used in this study were two different, following the formula $Ni_{50}Ti_{(50-x)}Hf_x$. Based on this configuration, the content of x= twelve in twelve hafnium (observing the substitutional character of hafnium compared to Titanium) in the alloy composition, thus guaranteeing a sufficient number of alloys with different compositions: $Ni_{50}Ti_{42}Hf_8$, $Ni_{50}Ti_{30}Hf_{20}$.

The solidification method used in this work is the fusion of alloys by arc melting; the technical specifications of the equipment used are maximum power of 18.5 kW; maximum current of the order of 400 A; a volume of 18 liters; 0.01 Pa vacuum, argon gas purge, and 0.12 MPa maximum pressure. The maximum melting temperature is around 3726.85 °C.

To avoid any presence of oxygen in the alloy, due to the affinity of this element with titanium, the following procedures were carried out: (i) the melting chamber was evacuated to 0.00133 Pa three consecutive times. In the last purge, argon gas was pressurized to 91192.5 Pa; (ii) shortly after, three fusions were made in a titanium getter, in an evacuated environment at 50622.5 Pa, before the final melting of the Ni-Ti-Hf bulk.

In this work, the DSC characterizations were performed using different heating runs in order to investigate the kinetics of the thermally activated phase transformation process. Observing this purpose, the controlled heating rates used were four, in the order: 2.5 (°C/min.); 5.0 (°C/min.); 10.0 (°C/min.); 20.0 (°C/min.).

3. Results and Discussions

From the analyzes taken based on thermal characterizations via (DSC), as supported by the literature, an increase in TTs was observed as the hafnium content increased in the samples were prepared by arc melting. This increase in TTs becomes very clear as we analyze the data obtained for the $Ni_{50}Ti_{30}Hf_{20}$ composition, as will be seen more clearly in Table 1 later. Therefore, the transformation temperatures, as well as their increments, must be observed as an indication of

what characterizes the addition of a ternary component to an alloy in the nickel titanium system with the express purpose of transforming this SMA into an SMA with HTSMA[9,10,21]. This increase in transformation temperatures due to the increase in the element hafnium, in the composition of the alloys, is well expressed when comparing Figures 1 and 2.

3.1. Analysis of phase transformation enthalpies (ΔH)

After carrying out the DSC tests, with the curves described in Figures 3 and 4, the variation in the enthalpies of transformation was analyzed according to the variation in heating rates and alloy compositions as the ternary element content was increased, as shown in Table 2.

3.2. Obtaining kinetic parameters from the adapted Avrami model

Regarding Avrami's theory, as different scientific experiments were carried out in recent decades, it was observed the need for the adaptive character of the equation and the graphic modeling printed by[22]. Such adaptive models of character changes were necessary so that the model could analytically forge a more comprehensive range of macromolecular events. Avrami himself implemented some of these adaptations in[23].

Table 1. Transformation temperatures in Ni-Ti-Hf alloys obtained by arc melting, bulk samples.

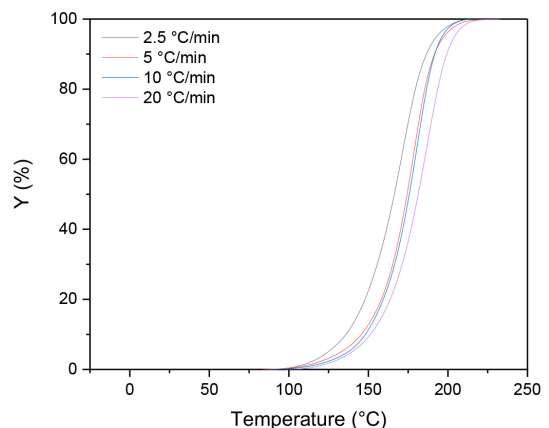| Composition	Heating rate (°C/min.)	Initial Temperature (°C)	Final Temperature (°C)
$Ni_{50}Ti_{42}Hf_8$	2.5	124.15	194.07
$Ni_{50}Ti_{42}Hf_8$	5.0	136.76	198.08
$Ni_{50}Ti_{42}Hf_8$	10.0	131.07	198.11
$Ni_{50}Ti_{42}Hf_8$	20.0	142.00	209.07
$Ni_{50}Ti_{30}Hf_{20}$	2.5	225.52	290.60
$Ni_{50}Ti_{30}Hf_{20}$	5.0	223.62	289.27
$Ni_{50}Ti_{30}Hf_{20}$	10.0	216.80	288.48
$Ni_{50}Ti_{30}Hf_{20}$	20.0	216.06	292.74

Figure 1. Descriptive sigmoid graph of the transformed fraction versus temperature, comparing the behavior of the transformations in alloy $Ni_{50}Ti_{42}Hf_8$, obtained by arc melting.
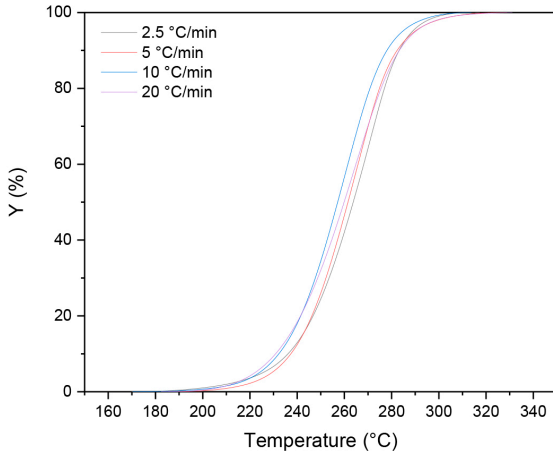
Effect of Heating Rate on the Kinetics of Martensitic Transformation of Ni-Ti-Hf alloys using Differential Scanning Calorimetry (DSC)

3

Figure 2. Descriptive sigmoid graph of the transformed fraction versus temperature, comparing the behavior of the transformations in the $Ni_{50}Ti_{30}Hf_{20}$ alloy, obtained by arc melting.

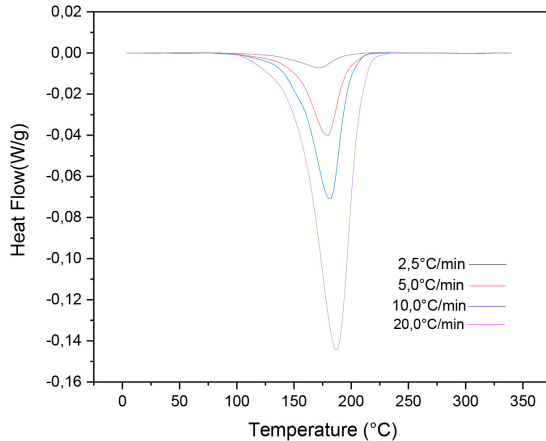**Figure 4.** Comparative graph of the DSC tests for the alloy of composition $Ni_{50}Ti_{30}Hf_{20}$, taking the different heating rates as a parameter.

Figure 3. Comparative Graph of the DSC tests for the alloy of composition $Ni_{50}Ti_{42}Hf_8$, taking the different heating rates as a parameter.

Table 2. Enthalpies of transformation obtained from the tests in (DSC) for the alloys obtained by arc melting.

Composition	Heating rate (°C/min.)	Transformation enthalpies (J/g)
$Ni_{50}Ti_{42}Hf_8$	2.5	0. 3036
$Ni_{50}Ti_{42}Hf_8$	5.0	1. 4009
$Ni_{50}Ti_{42}Hf_8$	10.0	2. 4558
$Ni_{50}Ti_{42}Hf_8$	20.0	5. 6529
$Ni_{50}Ti_{30}Hf_{20}$	2.5	0. 9088
$Ni_{50}Ti_{30}Hf_{20}$	5.0	2. 0231
$Ni_{50}Ti_{30}Hf_{20}$	10.0	4. 0148
$Ni_{50}Ti_{30}Hf_{20}$	20.0	6. 6713

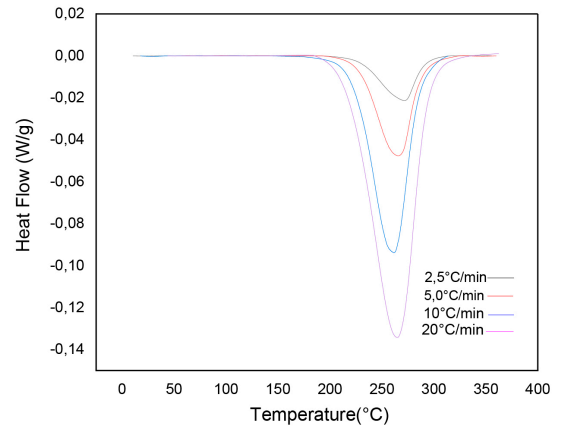From the point of view of calorimetric analysis, over the decades, other adaptations were made so that the theory,

initially developed in the case of changes of phases of solids in the isothermal state, was also efficient in the description of non-isothermal solids in the stage of changes phase[16,24-27].

Therefore, considering that the temperature varies during the test, gradually increasing or decreasing over time, and the material expresses kinetic transformations, Equation 1 can be written, used to guide the obtaining of the abscissa axes of the avrami model graphs obtained and expressed in Figures 5 and 6.

$$T = T_1 \pm \Phi \tau \qquad (1)$$

If T_1 refers to the temperature at the beginning of transformation (for $\tau=0$) and the sign is positive when the transformation takes place with constant heating and negative when the transformation takes place with constant cooling, the rate Φ defined as module $|dT/dt|$, So it is always positive[28]. To correlate the transformed fraction data as a function of time, considering the range of temperatures and time in which such transformations occur at constant rates (heating/cooling), the simplest model was used, similar to the first mathematical model described by Avrami[29]. In this work, a similar adapted form, as expressed by Equation 2.

Therefore, the adapted form of the JMAK models described was used[30]. Therefore:

$$x = 1 - \exp\left(-K' \tau^{n'}\right) \qquad (2)$$

Where x is the relative quantity transformed and τ, as expressed in Equation 2, refers to the time since the beginning of the non-isothermal thermoactivated transformation[28].

Therefore, the parameters of the Avrami Model contained in Tables 3 and 4 were obtained by performing the linear regression of a straight line obtained graphically, from the experimental data of x versus τ, through the relationship established by Equation 2.

When calling Y, the ordinate axis terms in graphs, this left member of linear regression equations is described as:

$$Y = ln\left[-\ln\left(1-x\right)\right] = \ln\left(ln\frac{1}{1-x}\right) \qquad (3)$$

Table 3. Kinetic parameters collected in the Avrami model Adapted to the $Ni_{50}Ti_{42}Hf_8$ alloy, obtained by arc melting, at different heating rates.

Φ (°C/min.)	Ln K'			n'		
		±	%		±	%
2.5	-4. 5882	0. 01073	0.23	1. 16421	0. 00332	0.28
5.0	-4. 6010	0. 01228	0.26	1. 18205	0. 00379	0.32
10.0	-4. 4897	0. 01166	0.26	1. 13976	0. 00366	0.32
20.0	-4. 5027	0. 00446	0.10	1. 17028	0. 00446	0.38

Table 4. Kinetic parameters collected in the Avrami model adapted for the $Ni_{50}Ti_{30}Hf_{20}$ alloy, obtained by arc melting, at different heating rates.

Φ (°C/min.)	Ln k'			n'		
		±	%		±	%
2.5	-4. 5217	0. 01282	0.28	1.18409	0. 00358	0.30
5.0	-4. 5115	0. 01356	0.30	1. 17363	0. 00383	0.32
10.0	-4. 4171	0. 0142	0.32	1. 18703	0. 00383	0.32
20.0	-4. 4316	0. 01962	0.44	1. 20104	0. 00525	0.43
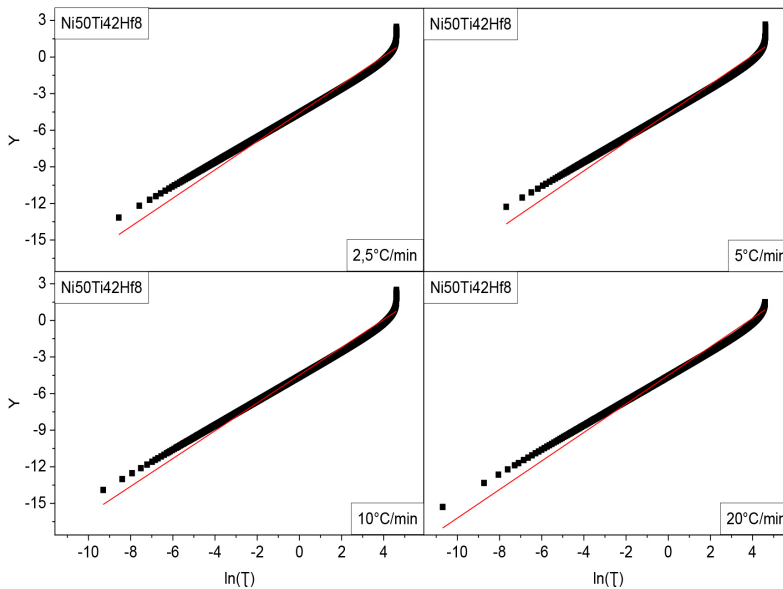
Figure 5. Graphs (Avrami-Adapted) for the composition $Ni_{50}Ti_{42}Hf_8$, in different experimental conditions (Bulks).

From the correlation between the ordered terms described by Y and the abscissa terms substantiated by τ, linear morphology graphs were obtained, characteristic of the Avrami model adapted to the non-isothermal case Figures 5 and 6, which, like Equation 2, present a substantial structural similarity with the graphs expressed in Avrami's initial theory applied to the isothermal case[29,30].

The results in (Tables 3 and 4) show an excellent fit in estimating the model parameters. The average uncertainty of Ln K' varies between 0.10% and 0.48%, and the average uncertainty of exponent n varies between 0.28% and 0.51%. These values presented using the adapted Avrami model are lower than the tolerable "experimental error" for DSC measurements, estimated at 5%[31]. This observed reality supported the suggestion that the Avrami model adapted to the non-isothermal case can correlate with the relative

experimental values - used for modeling. Therefore, it is a relevant tool as it mirrors empirical and theoretical aspects. These integrated experimental values, corresponding to the relative transformed phase y versus Τ for all compositions studied and at all heating rates used in the thermoactivated phase transformation event, were shown to be sufficiently expressed by the modeling as illustrated in Figures 5 and 6.

The graphs obtained by using the model are shown in Figures 5 and 6 and according to the theory, one of the descriptive measures of the model's efficiency as a method of translating empiricism is denoted by the proportion of the linear morphology presented and the proportion of this in relation to the total body expressed by the graph. At the end of the event, the points diverged from the usual behavior, indicating that the model presents some discrepancy between 98% and 100% of the relative transformed fraction.
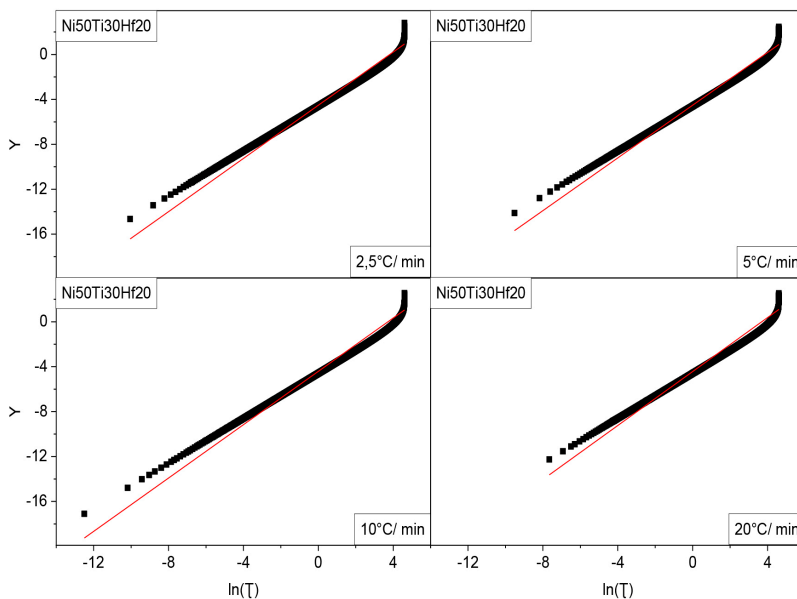
Figure 6. Graphs (Avrami-Adapted) for the composition $Ni_{50}Ti_{30}Hf_{20}$, in different experimental conditions (Bulks).

The observation of this result is also guided by the theory of maximum errors of prediction of empirical results expressed in[31], which admit as a "tolerable experimental error" for DSC measurements, the 5% level. This fact also reflects the practical idea that the adapted Avrami model represents a reasonable translation between what is empirically observed and the theoretical model adapted to translate its reality.

Regarding the kinetic parameters obtained, the results were consistent. Although in the adapted Avrami method, the physical meaning of events cannot be fully reached by such parameters since the non-isothermal method, totally equivalent to the isothermal Avrami method, is the Osawa method[27,32]. It was observed that the exponent obtained, around n=1, 13976 and n=1, 20104, are verified in interpretations of the application of Avrami's theories, which relates these exponents between n=1 and n=4 to different nucleation modes. It was also observed that the constancy in the values of n is due to the nature of the process studied being unique[27]. The transformation under constant heating from martensite to austenite, if other types of transformation were being observed, different values of n would be justifiable.

3.3. Activation Energies

Initially, it was based on the concept of transformed fraction, considering that this quantity provides substance in the analysis of the term apparent activation energy (Qap), obtaining these fractions. The apparent activation energy (Qap) for the martensite-austenite transformation can be calculated, observing that (Qap) starts from the values of the transformed fractions. The Arrhenius equation Equation 4. is an essential tool for synthesizing such concepts, enabling the analysis of activation energies depending on the fractions transformed at each instant[6,33,34]. Such equation was helpful for the present study concerning the description of the phase transformation process, translating as SMAS, absorbs activation energy (Qap) to develop its reversible phase transformations[19,21].

Table 5. Apparent activation energies obtained by the Arrhenius method for each composition and experimental condition.

Activation energies in (Kj/mol) for each composition and experimental condition		
Heating rate (°C/min.)	Q_{ap} $Ni_{50}Ti_{42}Hf_{8}$	Q_{ap} $Ni_{50}Ti_{30}Hf_{20}$
2.5	100.66	159.09
5.0	107.64	149.65
10.0	92.57	209.80
20.0	89.96	126.39

The simplest way to discretely find (Qap) for the martensite-austenite transformation, which was adopted in this work, as mentioned, was through the application of the Arrhenius equation, which can more succinctly describe the phenomenon of kinetic transformation at a given moment, through the following steps:

Application of the Arrhenius equation, describe in its most basic forms as described in Equation 4:

$$r = A.\exp\left(\frac{-Q_{ap}}{RT}\right) \tag{4}$$

Therefore, considering that the transformation rate follows an Arrhenius equation as mentioned in Equation 4. Thus, the graphs were created with ln(rate) in s-1 against the inverse temperature (1/T) at each point, which gave approximately a straight line, where the slopes give (-Qap/R), as can be seen in Figures 7 and 8. Since R, the ideal gas constant, is a known value, the apparent activation energy (Qap) values were calculated[35,36].

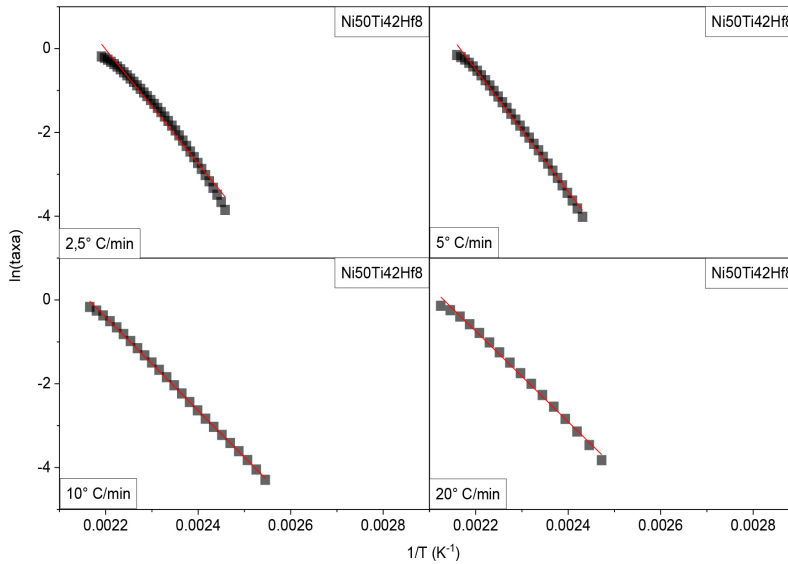From this criterion and the conventions for the Arrhenius equations discussed in[30] Table 5 was obtained.

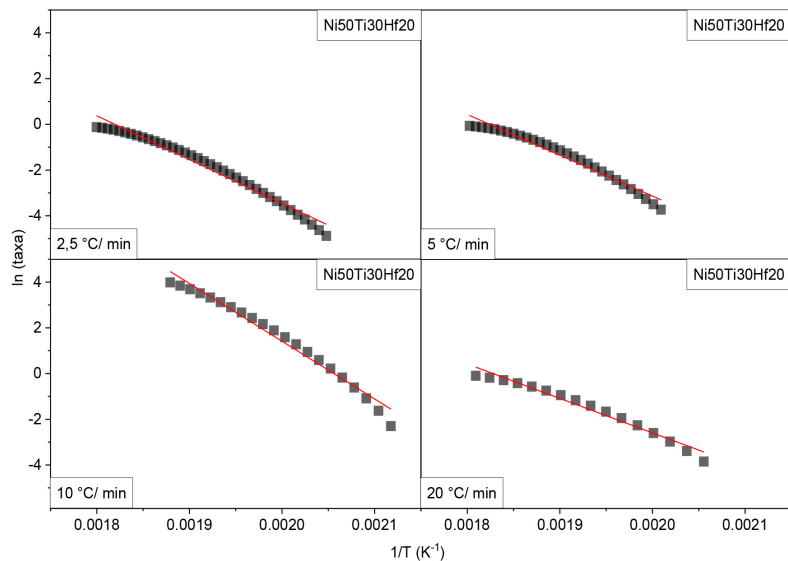**Figure 7.** Arrhenius plots for the $Ni_{50}Ti_{42}Hf_8$ composition, under different experimental conditions (Bulks).

Figure 8. Arrhenius plots for the composition $Ni_{50}Ti_{30}Hf_{20}$, under different experimental conditions (Bulks).

Observing the activation energies Table 5 in comparison with the transformation enthalpies data obtained by the empirical method of capturing DSC tests Table 2, it is noted that in these first collected (empirical) data, a direct correlation was observed both between the increase in the amount of the ternary element hafnium in the composition, and the heating rates with the increase in transformation enthalpies. Furthermore, using the Arrhenius mathematical and kinetic model, it was observed from the data expressed in Table 5, that they only managed to capture the influence of increasing the amount of the ternary element hafnium on the increase in activation energies. The fact of this increase in activation energies, as the content of a certain element in the initial compositions increases, is corroborated by the literature, and

also its decrease in some cases, depending on the method of obtaining the alloys and their processing history[37]

4. Conclusions

1. The experimentally obtained transformation enthalpies reflected the thermal activity, as they increased proportionally with the increase in heating rates.

2. With the increase in the amount of the element hafnium in the composition of the alloy, there was a proportional increase in the transformation enthalpies. This fact also materialized in the activation energies (Qap) theoretically obtained using the Arrhenius model.

Effect of Heating Rate on the Kinetics of Martensitic Transformation of Ni-Ti-Hf alloys using Differential Scanning Calorimetry (DSC)

7

3. Transformation temperatures increased proportionally to add the ternary element hafnium to the alloy composition.

4. The increases observed in the activation energies of the alloys as the ternary element hafnium was added, denoting that the larger atomic diameter and the higher melting temperature of hafnium induce a more significant energy barrier to be overcome.

5. The adapted Avrami method proved to be an efficient tool for describing the phenomenon of phase transformation since the dispersion measures generated were quite acceptable. The average uncertainty of ln K' varies between 0.10% and 0.44%, and the average uncertainty of exponent n varies between 0.28% and 0.43%.

6. The adapted Avrami model obtained a value of n (Avrami exponent) consistent with Avrami's theory for the type of nucleation occurring in martensite-austenite transformations.

7. The Arrhenius kinetic model (from the apparent activation energies obtained) captured the influence of increasing the amount of the ternary element hafnium on the increment of activation energies.

5. References

1. Fang H, Wong B, Bai Y. Kinetic modelling of thermophysical properties of shape memory alloys during phase transformation. Constr Build Mater. 2017;131:146-55. http://doi.org/10.1016/j.conbuildmat.2016.11.064.

2. Otsuka K, Ren X. Physical metallurgy of Ti-Ni-based shape memory alloys. Prog Mater Sci. 2005;50(5):511-678. http://doi.org/10.1016/j.pmatsci.2004.10.001.

3. Rao A, Srinivasa AR, Reddy JN. Design of shape memory alloy (SMA) actuators. Cham: Springer; 2015. http://doi.org/10.1007/978-3-319-03188-0.

4. Dzogbewu TC, de Beer DJ. Additive manufacturing of NiTi shape memory alloy and its industrial applications. Heliyon. 2024;10(1):e23369. http://doi.org/10.1016/j.heliyon.2023.e23369.

5. Poitout DG, editor. Biomechanics and biomaterials in orthopedics. 2nd ed. London: Springer; 2016. 547 p. http://doi.org/10.1007/978-1-84882-664-9.

6. Zuo S, Wu R, Pang G, Yang Y, Jin M. High temperature internal friction in $Ni_{50.3}Ti_{29.7}Zr_{20}$ shape memory alloy. Intermetallics. 2019;109:174-8. http://doi.org/10.1016/j.intermet.2019.04.006.

7. Lagoudas DC. Shape memory alloys: modeling and engineering applications. New York: Springer; 2008. http://doi.org/10.1007/978-0-387-47685-8.

8. Shuitcev A, Ren Y, Sun B, Markova GV, Li L, Tong YX, et al. Precipitation and coarsening kinetics of H-phase in NiTiHf high temperature shape memory alloy. J Mater Sci Technol. 2022;114:90-101. http://doi.org/10.1016/j.jmst.2021.11.011.

9. Coughlin DR, Phillips PJ, Bigelow GS, Garg A, Noebe RD, Mills MJ. Characterization of the microstructure and mechanical properties of a 50.3Ni–29.7Ti–20Hf shape memory alloy. Scr Mater. 2012;67(1):112-5. http://doi.org/10.1016/j.scriptamat.2012.03.036.

10. Jiang M, Chen X, Nurly HF, Yang X, Liu Y, Cai Y, et al. Hot deformation behavior of $Ni_{50.4}Ti_{34.6}Hf_{15}$ high-temperature shape memory alloy. J Mater Res Technol. 2024;28:1165-76. http://doi.org/10.1016/j.jmrt.2023.12.084.

11. Meng XL, Cai W, Wang LM, Zheng YF, Zhao LC, Zhou LM. Microstructure of stress-induced martensite in a Ti-Ni-Hf high temperature shape memory alloy. Scr Mater. 2001;45(10):1177-82. http://doi.org/10.1016/S1359-6462(01)01147-2.

12. Ma YQ, Jiang CB, Feng G, Xu HB. Thermal stability of the $Ni_{54}Mn_{25}Ga_{21}$ Heusler alloy with high temperature transformation. Scr Mater. 2003;48(4):365-9. http://doi.org/10.1016/S1359-6462(02)00450-5.

13. Meng XL, Zheng YF, Cai W, Zhao LC. Two-way shape memory effect of a TiNiHf high temperature shape memory alloy. J Alloys Compd. 2004;372(1–2):180-6. http://doi.org/10.1016/j.jallcom.2003.10.020.

14. Khalil-Allafi J, Daneshvar H, Safavi MS, Khalili V. A survey on crystallization kinetic behavior of direct current magnetron sputter deposited NiTi thin films. Physica B. 2021;615:413086. http://doi.org/10.1016/j.physb.2021.413086.

15. Evirgen A, Karaman I, Santamarta R, Pons J, Noebe RD. Microstructural characterization and shape memory characteristics of the $Ni_{50.3}Ti_{34.7}Hf_{15}$ shape memory alloy. Acta Mater. 2015;83:48-60. http://doi.org/10.1016/j.actamat.2014.09.027.

16. Yi X, Sheng L, Fu G, Sun K, Yang Q, Wang H, et al. Insights into the martensitic transformation kinetics and mechanical properties of quaternary Ti-Ni-Nb-V shape memory alloys. J Mater Res Technol. 2022;19:557-65. http://doi.org/10.1016/j.jmrt.2022.05.084.

17. Oliveira AB, Peixoto EB, Duque JGS, Silva LS, Silva RAG. Bainite precipitation in a Cu–Al–Mn-Gd shape memory alloy. Materialia. 2021;16:101101. http://doi.org/10.1016/j.mtla.2021.101101.

18. Lad KN, Savalia RT, Pratap A, Dey GK, Banerjee S. Isokinetic and isoconversional study of crystallization kinetics of a Zr-based metallic glass. Thermochim Acta. 2008;473(1–2):74-80. http://doi.org/10.1016/j.tca.2008.04.011.

19. Tian X, Wang Z, Zhu J, Tan C, Zhang K, Yu Z, et al. The effect of Fe doping on the crystallization kinetics of Ni-Mn-Sn free-standing alloy thin films. J Non-Cryst Solids. 2018;495:19-26. http://doi.org/10.1016/j.jnoncrysol.2018.05.008.

20. Aghajani Derazkola H, Garcia E, Murillo-Marrodán A, Conde Fernandez A. Review on modeling and simulation of dynamic recrystallization of martensitic stainless steels during bulk hot deformation. J Mater Res Technol. 2022;18:2993-3025. http://doi.org/10.1016/j.jmrt.2022.03.179.

21. Inaekyan K, Brailovski V, Prokoshkin S, Korotitskiy A, Glezer A. Characterization of amorphous and nanocrystalline Ti-Ni-based shape memory alloys. J Alloys Compd. 2009;473(1-2):71-8. http://doi.org/10.1016/j.jallcom.2008.05.023.

22. Mukherjee T, Elmer JW, Wei HL, Lienert TJ, Zhang W, Kou S, et al. Control of grain structure, phases, and defects in additive manufacturing of high-performance metallic components. Prog Mater Sci. 2023;138:101153. http://doi.org/10.1016/j.pmatsci.2023.101153.

23. Avrami M. Kinetics of phase change. II Transformation-time relations for random distribution of nuclei. J Chem Phys. 1940;8(2):212-24. http://doi.org/10.1063/1.1750631.

24. Zhou ZN, Yang L, Li RC, Li J, Hu QD, Li JG. Martensitic transformations and kinetics in Ni-Mn-In-Mg shape memory alloys. Intermetallics. 2018;92:49-54. http://doi.org/10.1016/j.intermet.2017.09.016.

25. Qiao JC, Pelletier JM. Isochronal and isothermal crystallization in Zr 55Cu 30Ni 5 Al 10 bulk metallic glass. Trans Nonferrous Met Soc China. 2012;22(3):577-84. http://doi.org/10.1016/S1003-6326(11)61216-8.

26. Kozmidis-Petrović AF, Lukić SR, Štrbac GR. Calculation of non-isothermal crystallization parameters for the $Cu_{15}(As_2Se_3)_{85}$ metal-chalcogenide glass. J Non-Cryst Solids. 2010;356(41-42):2151-5. http://doi.org/10.1016/j.jnoncrysol.2010.08.026.

27. Wang K, Chen L. Crystallization kinetics of $Sb_{70}Se_{30}$ thin films for phase change memories under the non-isothermal conditions. J Cryst Growth. 2023;624:127434. http://doi.org/10.1016/j.jcrysgro.2023.127434.

28. Zotov N, Marzynkevitsch V, Mittemeijer EJ. Evaluation of kinetic equations describing the martensite-austenite phase

transformation in NiTi shape memory alloys. J Alloys Compd. 2014;616:385-93. http://doi.org/10.1016/j.jallcom.2014.07.148.

29. Avrami M. Kinetics of phase change. I: general theory. J Chem Phys. 1939;7(12):1103-12. http://doi.org/10.1063/1.1750380.

30. Hong SH, Park HJ, Song G, Liaw PK, Kim KB. Ultrafine shape memory alloys synthesized using a metastable metallic glass precursor with polymorphic crystallization. Appl Mater Today. 2021;22:100961. http://doi.org/10.1016/j.apmt.2021.100961.

31. Kasper M. G.W.H. Hohne, W.F. Hemminger, H.-J. Flammersheim: differential scanning calorimetry. Anal Bioanal Chem. 2004;380(3):366-7. http://doi.org/10.1007/s00216-004-2814-8.

32. Arman M, Shahri F, Gholamipour R. Effect of Al doping on the kinetics of reverse martensitic transformation in Ni-Mn-In Heusler alloys. Mater Sci Eng B. 2024;300:117068. http://doi.org/10.1016/j.mseb.2023.117068.

33. Camuffo D. Consequences of the Maxwell–Boltzmann distribution. In: Camuffo D. Microclimate for cultural heritage: conservation, restoration, and maintenance of indoor and outdoor monuments. Amsterdam: Elsevier; 2014. p. 347-66. http://doi.org/10.1016/B978-0-444-63296-8.00010-X.

34. Martins CB Jr, Silva R, Gargarella P, Gleeson B, Rovere CAD. Characterization of $NiTiNb_{10.5}$ shape memory alloy: microstructural aspects and high-temperature oxidation behavior. Corros Sci. 2023;225:111627. http://doi.org/10.1016/j.corsci.2023.111627.

35. Pandolfi GS, Martins SC, Buono VTL, Santos LA. Precipitation kinetics of Ti3Ni4 and multistage martensitic transformation in an aged Ni–rich Ni–Ti shape memory alloy. J Mater Res Technol. 2020;9(4):9162-73. http://doi.org/10.1016/j.jmrt.2020.06.046.

36. Khazaei Feizabad MH, Khayati GR, Minouei H. A kinetic study approach for in-situ preparation of amorphous Ni based nanocomposite reinforced by nanocrystalline Ni-Ti shape memory alloy. J Non-Cryst Solids. 2019;524:119652. http://doi.org/10.1016/j.jnoncrysol.2019.119652.

37. Banerjee S, Robi PS, Srinivasan A. Calorimetric study of precipitation kinetics of Al-Cu-Mg and Al-Cu-Mg-0.06 wt.% Sn alloys. Met Mater Int. 2010;16(4):523-31. http://doi.org/10.1007/s12540-010-0802-4.